Diffuse optical imaging of brain activation: approaches of optimizing image sensitivity, resolution and accuracy
David A. Boas *et al.*

**NeuroImage (2004)**

**Presenter : Evgenii Kim**

GIST, Dept. of Information and Communication

Gwangju Institute of Science and Technology





# Outline

- Introduction
- Diffuse optical imaging forward and inverse problem basics
- Optimum wavelengths and cross-talk in estimating hemoglobin concentrations
- Systemic physiological signal interference
- Improving image resolution with overlapping measurements
- MRI structural and functional spatial priors for improving quantitative accuracy of DOI
- Conclusion

# Introduction

- Near – infrared spectroscopy (NIRS) and diffuse optical imaging (DOI) are techniques applied to study neural activity in the brain.
- Infrared light is composed of a broad range of electromagnetic waves from 770 nm to 1 mm.

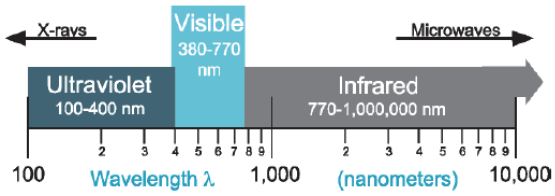


http://www. en.wikipedia.org/



# Introduction

- Optical Window

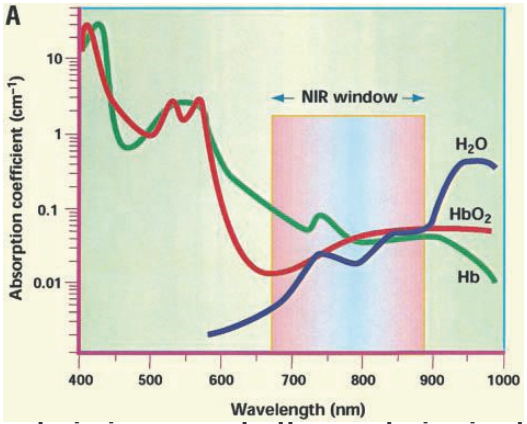


Hemoglobin is the iron-containing metalloprotein in the red blood cells.

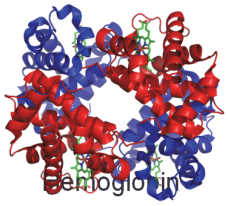


http://www. en.wikipedia.org/

# Introduction

- Using NIRS we can get:
  - concentrations of oxyhemoglobin ($HbO_2$)
  - concentrations of deoxyhemoglobin ($HbR$)
  - regional blood volume
  - blood flow
  - metabolic rate of oxygen consumption
- This ability is potentially important for a brain studies particularly



# Introduction

- Limitation:
  - Estimation of $HbO_2$ and $HbR$ concentrations is sensitive to random measurement and systematic errors appeared from incorrect model parameters.
  - The sensitivity to brain activation is able to decrease due to contamination from several systemic physiological signals

# Diffuse optical imaging forward and inverse problem basics

- Diffusion Equation

$$\nabla \cdot D(r)\nabla\Phi(r,t) - v\mu_a(r)\Phi(r,t) + vS(r,t) = \frac{\partial\Phi(r,t)}{\partial t}$$

where $\Phi(r,t)$ photon fluence rate

$$\Phi(r,t) = vU(r,t)$$

*D(r)* photon diffusion coefficient

$$D = v/3(A = \mu'_s + \mu_a);\ \mu'_s = (1-g)\mu_s$$

*S(r,t) isotropic source*



# Monte Carlo Simulation

For REF

- Monte Carlo methods are a class of computational algorithms that rely on repeated random sampling to compute their results.
- The path of each photon packet is determined by the sampling of random numbers and a set of functions or probability distributions describing the likeliness of for example the step length and scattering angles.
- This way of stochastic simulation relies on the simulation of a large number of photon packets and the solutions provided are more or less noisy depending on the number of photons simulated.

# Solutions of the Diffusion Equation for Comparison with Monte Carlo

For REF

$$\Phi(r_s, r_d, t) = \frac{vS}{4\pi D}\left[\exp\left(-\frac{|r_s - r_d|^2}{(4Dt)}\right) - \exp\left(-\frac{|r_{s,i} - r_d|^2}{(4Dt)}\right)\right]\exp(-v\mu_a t)$$

where $r_d$ the detector position at time $t$, generated by a point source of amplitude $S$ at position $r_s$. The position of the image source is indicated by $r_{s,i}$.



# The modified Beer-Lamber law

- $\Delta OD_i(t,\lambda) = -\log\left(\frac{\Phi(t,\lambda)}{\Phi_0(\lambda)}\right) = \sum_{j=1}^{N_{vox}} \Delta\mu_{a,j}(t,\lambda) L_{i,j}(\lambda)$

where $OD$ is the attenuation measured in optical densities; $\Phi_0$ is average detected photon fluence; $L_{i,j}$ is the effective pathlength of detected photons for *i*th measurement in the *j*th voxel.

$$\mu_a(\lambda) = \varepsilon_{HbO_2}(\lambda)[HbO_2] + \varepsilon_{HbR}(\lambda)[HbR]$$

$$\begin{pmatrix}\Delta[HbR]\\ \Delta[HbO_2]\end{pmatrix} = \frac{1}{L}\begin{pmatrix}\varepsilon_{HbR}^{\lambda_1} & \varepsilon_{HbO_2}^{\lambda_1}\\ \varepsilon_{HbR}^{\lambda_2} & \varepsilon_{HbO_2}^{\lambda_2}\\ \hdashline \varepsilon_{HbR}^{\lambda_n} & \varepsilon_{HbO_2}^{\lambda_n}\end{pmatrix}^{-1}\begin{pmatrix}\Delta OD^{\lambda_1}\\ \Delta OD^{\lambda_2}\\ \hdashline \Delta OD^{\lambda_n}\end{pmatrix}$$

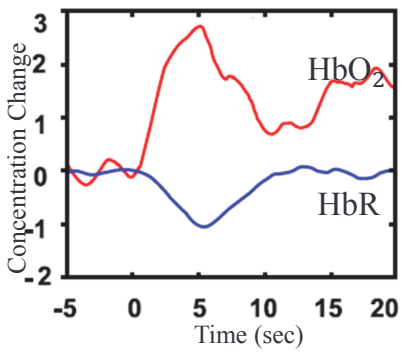

# Optimum wavelengths and cross-talk in estimating hemoglobin concentrations

- Most published optical results show us that two wavelengths can provide sufficient accuracy.
- Judicial choice of measurement wavelengths is required, because it can partially reduce random measurement, systematic errors (690 or 750 with 830 nm) and cross-talk in the estimate of the $HbO_2$ and $HbR$ concentrations (780 and 830 nm).
- It is important to choose a wavelength above and below the hemoglobin isobestic point at 805 nm.



# Systemic physiological signal interface

- The system has numerous sources of systemic signal interference that reduce its sensitivity to weaker brain activation signals.
- To improve the optical sensitivity to brain activation it is required to use special signal processing methods that distinguish the different source signals in space and time. Some research used a principle component analysis (PCA)

# Principle component analysis

For REF

- PCA is a way of identifying patterns in data, and expressing the data in such a way as to highlight their similarities and differences.
- The main advantage of PCA is that once you have found these patterns in the data, you can compress the data, by reducing the number of dimensions.

Lindsay I Smith, 2002



# Using PCA

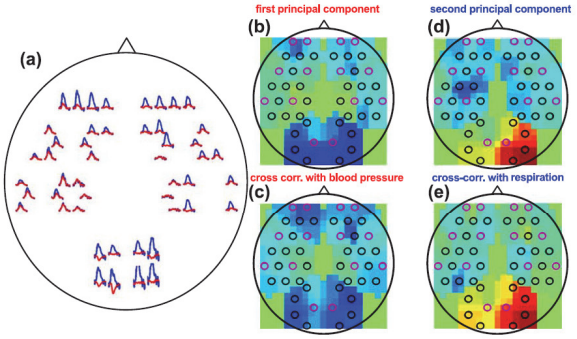


Fig. 3. (a) Spatial-temporal map of brain activation in response to 10 blocks of right hand finger tapping. The blue curves are the $\Delta$OD changes at 830 nm block averaged after a temporal band-pass filter between 0.02 and 0.8 Hz; the red curves are the $\Delta$OD changes obtained after PCA analysis. The $x$-axis is 35 s long, with the stimulation period lasting for 10 s, followed by 20 s of baseline. The $y$-axis is from $-7\%$ to 7% changes in $\Delta$OD. (b) and (d) Maps of the first and second principal component of the optical data at 830 nm obtained during 300 s of baseline. (c) and (e) Cross-correlation maps of the optical data with the blood pressure (c) and respiration (e) during baseline. The optical data was cross-correlated with blood pressure and respiration with a 2-s lag.

# MRI structural and functional spatial priors for improving quantitative accuracy of diffuse optical imaging

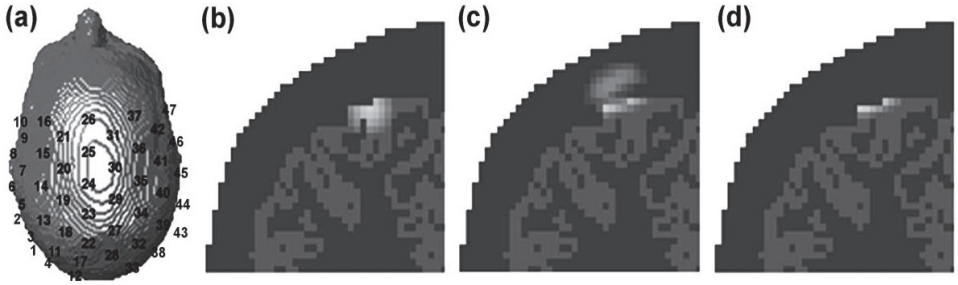


Fig. 5. Comparison of image reconstruction with and without a cortical constraint. (a) Probe geometry on a 3D segmented head. (b) True location of the simulated absorption change. (c) Image reconstructed using DOT and overlapping measurements. (d) Image reconstructed with a cortical constraint.



# Temporal correlation of *f*MRI and DOI

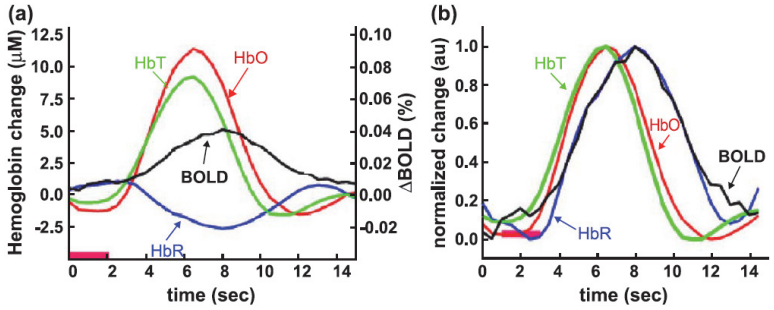


Fig. 6. (a) Response functions of hemoglobin concentrations and BOLD for event-related finger tapping as measured through simultaneously acquired fMRI–BOLD and DOI optical recordings of the primary motor cortex. (b) Normalized and rescaled response functions for the event-related finger tapping to allow visualization of the four variables on the same linear scale. The deoxyhemoglobin data have also been inverted to emphasize the strong correlation between deoxyhemoglobin and BOLD.

# Spatial correction of *f*MRI and DOI

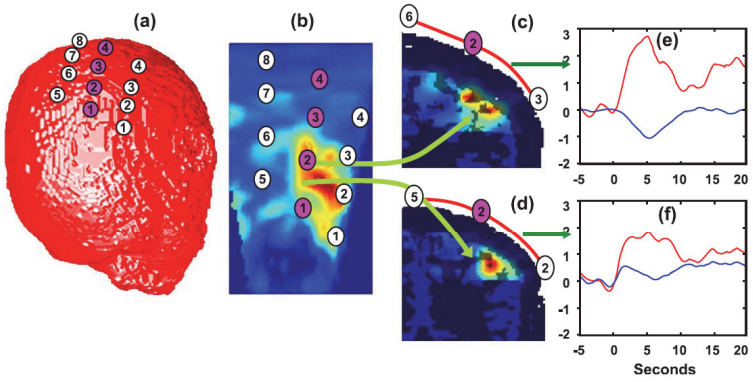


Fig. 7. (a) Coregistration of the position of optical sources (pink) and detectors (white) on the structural MRI of the subject. (b) Maximum intensity radial projection of the fMRI *t* statistic image on to the scalp. The source and detector positions are overlaid to reveal the spatial correlation of the optical signals and the BOLD signal. (c) and (d) Coronal slices through the maximum fMRI response (d) and 1 cm posterior (c). (e) and (f) Hemoglobin concentration time traces measured with source 2 and detectors 3 and 2, respectively, in relative units. Red oxyhemoglobin, blue deoxyhemoglobin. The stimulus starts at $t = 0$ s and lasts 2 s.



# Conclusion

- NIRS gives us enough function information about tissue, to be widely used in the study of human brain.
- In addition, the extension of NIRS to DOI will improve the sensitivity, resolution and accuracy of the optical estimates of the hemodynamic response to brain activation

# References


- Boas D.A., Dale M., Franceschili M. A., 2004. Diffuse optical imaging of brain activation: approaches of optimizing image sensitivity, resolution and accuracy. NeuroImage 23(2004), 275-288
- Boas, D.A., Culver, J., Stott, J., Dunn, A.K., 2002. Three dimensional Monte Carlo code for photon migration through complex heterogeneous media including the adult head. Opt. Express 10, 159– 170.
- Smith L. I., 2002, A tutorial on Principal Components Analysis.

**Title: Direct recording of holograms by a CCD target and numerical reconstruction**

U.Schnars and W.Juptner

Presenter: Nitin Rawat
Date: 4/9/2013

Here they introduced a method that uses a charge-coupled device detector (CCD) as a holographic recording medium. However, using CCD's for recording holograms is advantageous and no chemical or physical developing is necessary. Reconstruction can be performed by digital image processing.

In this Note, the mathematical reconstruction is done directly with the digitally sampled Fresnel hologram form the CCD.

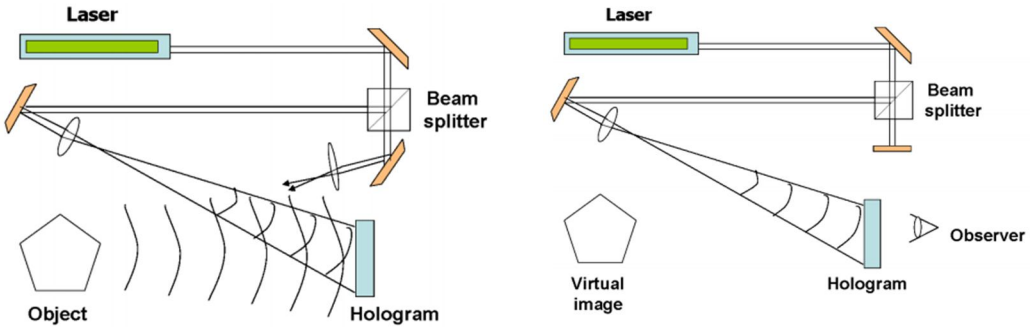


The holographic process is described mathematically as follows:

$$O(x,y) = o(x,y)\,\mathrm{e}^{i\varphi_o(x,y)} \quad \text{... (1.1)}$$

Is the complex amplitude of the object wave with real amplitude o and phase $\varphi_o$ and

$$R(x,y) = r(x,y)\,\mathrm{e}^{i\varphi_R(x,y)} \quad \text{... (1.2)}$$

Is the complex amplitude of the reference wave with real amplitude r and phase $\varphi_R$

$$I_H(x,y) = \left|O(x,y) + R(x,y)\right|^2$$

$$= (O(x,y) + R(x,y))(O(x,y) + R(x,y))^*$$

$$= R(x,y)R^*(x,y) + O(x,y)O^*(x,y)$$

$$+ O(x,y)R^*(x,y) + R(x,y)O^*(x,y) \quad \text{... (1.3)}$$

$$I_H(x,y) = \left|R\right|^2 + \left|O\right|^2 + R^*O + RO^* \quad \text{... (1.4)}$$

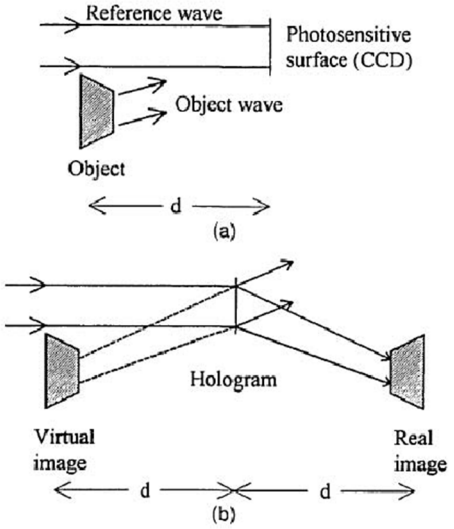


Fig. 1. Off-axis holography with a plane reference wave: (a) recording, (b) reconstruction.

Fig.1 (a) shows the recording geometry. A plane reference wave and the diffusely reflected object wave are interfering at the surface of a photosensitive medium.

In optical holography the object wave can be reconstructed by illumination of the processed hologram with a plane wave, similar to that used in the process of recording.

Looking through the hologram, one notice a virtual image of the object at the position of the original object $[Fig.1(b)]$ .If a screen is placed at a distance *d* behind the hologram, a real image is formed.

Mathematically the amplitude and phase distribution in the plane of the real image can be found by the Fresnel-Kirchhoff integral.

Fresnel integral of the digitized hologram intensity $I_H(k,l)$ :-

$$\Psi(m,n) = A\exp\left[\frac{i\pi}{\lambda d}\left(m^2\Delta\xi^2 + n^2\Delta\eta^2\right)\right] \times FFT\left\{R_D(k,l)I_H(k,l)\times\exp\left[\frac{i\pi}{\lambda d}\left(k^2\Delta x^2 + l^2\Delta y^2\right)\right]\right\}_{m,n}$$

Where k, l, m, n $(-N/2 \le k,l \le N/2)$ are integers; FFT is the fast Fourier transform operator; d is the distance between the hologram and the observation plane; and $A = \exp(i2\pi d/\lambda)/(i\lambda d)$ is a constant.

$\Delta x = \Delta y = L/N$ define the sampling intervals in the observation plane ( $\Delta\xi$ and $\Delta\eta$ ) are related to the size of the CCD (L) and to the distance d by the following relation:

$$\Delta\xi = \Delta\eta = \lambda d/L$$

The reconstructed wave front is an array of complex numbers. An amplitude-contrast image and a phase-contrast image can be obtained by calculation of the intensity

$\left[\mathrm{Re}(\psi)^2 + \mathrm{Im}(\psi)^2\right]$ and the argument $\left\{a\tan\left[\mathrm{Re}(\psi)/\mathrm{Im}(\psi)\right]\right\}$ of $\psi(m,n)$, respectively.

$\Psi(m,n)$ is a matrix of N x N points that describes the amplitude and phase distribution of the real image.

$\Delta\xi$ and $\Delta\eta$ are the pixel sizes in the reconstructed image. If only the intensity distribution according to Eq.3 is of interest, the phase factor before the summation can be neglected.

In the experimental investigations a CCD array is placed at the position of the photosensitive surface (Fig.1).

The CCD array consists of 1024 x 1024 pixels. The pixel area(L) is $6.8\mu m \times 6.8\mu m$.

For computation the hologram is stored in a digital image processing system. The object in this experiment was a cube with a side of length of 11 mm, which was placed at a distance of 1 m from the target.

A helium-neon laser was used as a light source.

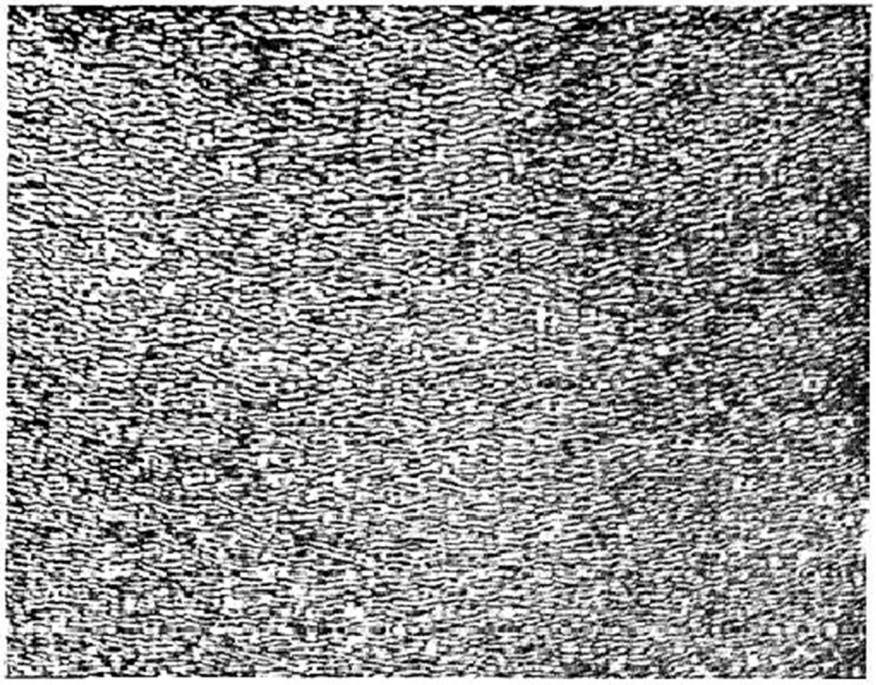

Fig. 2. Digitally sampled off-axis hologram.

Fig. 2 shows a part of a digitally sampled hologram. The original dimensions of the whole hologram were 7mm x 7mm, which are the dimensions of the CCD chip.

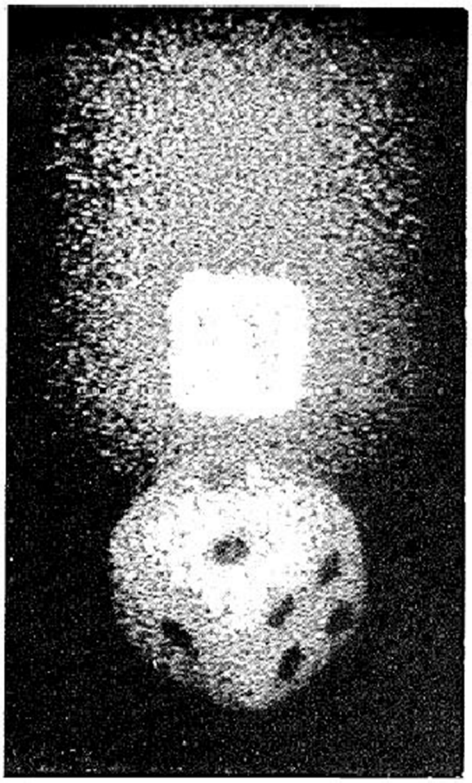

Fig. 3. Numerical reconstruction.

The numerical reconstruction according to $\Psi(m,n)$ is demonstrated in Fig.3. A real image of the cube together with the undiffracted reference wave is noticeable.

Because of the off-axis geometry, these two parts of the real image are separated. Furthermore, a speckle appearance on the reconstructed cube is noticeable. It is a result of the interaction between coherent light and the rough surface of the object.

# Localisation of cognitive tasks used in EEG-based BCIs

**M. Dyson *, F. Sepulveda, J.Q. Gan**

**Clinical Neurophysiology (2010.3)**

**Presenter : Younghak Shin**

GIST, Dept. of Information and Communication, INFONET Lab.

Gwangju Institute of Science and Technology





## Objective

- In BCIs, motor and non-motor(e.g., auditory) cognitive states are used.
- To provide candidate electrode sites and neurophysiological reference information used in brain–computer interfacing research, they investigate six cognitive tasks.
- This is the first study to provide candidate electrode sites for multiple tasks used in brain–computer interfacing

# Methods

- Cognitive tasks

- Six cognitive tasks were tested against the idle state
- The idle state was used as a baseline against each task in order to observe changes in the activation associated

1. Arithmetic
- Subtraction was selected as an arithmetic task
- Generate a three digit number and a single digit number for each trial
- The single digit number was to be repeatedly subtracted from the results of each calculation
- continuing for the duration of the trial.

2. Navigation imagery
- Subjects were instructed to select a familiar route between two locations
- Subjects were required to bring to mind images associated with the route.





# Methods

3. Auditory recall
- Auditory recall involved recall of a tune familiar to subjects
- and involved the mental rehearsal of the said song.

4. Phone imagery
- This task was an alternative auditory task
- and involved subjects bringing to mind a familiar telephone bell or ringtone and retain the sound for the duration of the trial
- It was emphasized that this was an auditory task and associations should not be made with motor activities associated with telephone use

5. Motor imagery of the left hand
- A wrist extension was demonstrated to subjects.
- Motor imagery was defined as bringing to mind these associations without performing the task itself

6. Motor imagery of the right hand
- Instructions matched those for left hand motor imagery.

# Methods

- Data collection

- Subjects : Seven male subjects (age 24–35) took part in the study. All subjects were able bodied, free from medication and any disorders of, or injuries to the central nervous system.
- Protocol
  - Each run contained 10 trials (randomly ordered)
  - trials within each run were split equally between the active task condition and the idle condition.
  - Each run was repeated six times, producing 30 trials for each mental task and 30 trials of associated idle data.
  - The number of runs per session was dependent on subject preference.
  - Within each run cues appeared after a 60 s pre-trial period

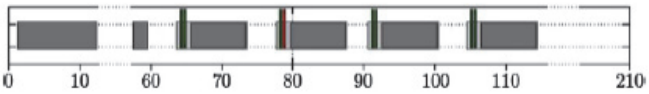


Fig. 1. Outline of an experimental run with time in seconds. A breakdown of the components of a trial are shown in Fig. 2.





# Methods

- Protocol
  - A trial began with the presentation of a fixation cross in the centre of the screen.
  - Paired beep sounds were used to cue the active task condition and the idle task.
  - Two 70 ms duration tones were presented
  - The first sound was consistently 1 kHz, the second either 1 or 1.3 kHz.
  - If the two tones were perceived as the same tone the subject performed the given mental task for the run
  - If the tones were different the subject relaxed for the duration of the trial
  - Subjects were instructed to attempt to perform each task until the fixation cross disappeared from the screen

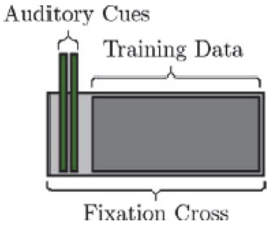


Fig. 2. Breakdown of the components of a trial as used in Fig. 1.

# Methods

- Recordings
  - EEG was recorded from 64 electrodes positioned according to the international 10–20 layout using a BioSemi Active2 system.
  - EEG signals were filtered between 0.1 Hz and 100 Hz (Butterworth–Order 5)
  - Data were sampled at a frequency of 256 Hz

- Feature extraction
  - Features were extracted in two representations, band power and reflection coefficients.
  - Band power extraction was performed on 10 frequency bands, corresponding to the delta (0.1–5 Hz), theta (5–8 Hz), alpha (8–12Hz), sigma (12–15 Hz), beta (15–25 Hz) bands and the five bands in the gamma range (25–35, 35–45, 45–55, 55–65, 65–75 Hz).
  - Features were extracted for each band on each channel, giving a total of 640 features based on band power.





# Methods

- Feature extraction
  - Reflection coefficients, or partial correlation (PARCOR) coefficients, are obtained via autoregressive analysis and are related to autoregression coefficients
  - An autoregressive model represents a time signal as an output of an all pole filter driven by white noise.
  - Filter coefficients are calculated from a block of samples as input signal

The notation AR($p$) indicates an autoregressive model of order $p$. The AR($p$) model is defined as

$$X_t = c + \sum_{i=1}^{p} \varphi_i X_{t-i} + \varepsilon_t$$

where $\varphi_1, \ldots, \varphi_p$ are the parameters of the model, $c$ is a constant, and $\varepsilon_t$ is white noise.

# Methods

- Feature selection
  - A sequential forward floating search (SFFS) *[Pudil et al. 1994]* algorithm was used to obtain electrode-feature combinations for each subject-task dataset.
  - The algorithm works on the extracted feature space Y, which contains a finite number of features, D: $Y = \{y_j \mid j = 1,\ldots,D\}$.
  - Output is a subset of extracted features X, consisting of the *k* features producing best discrimination in the feature space:

$$X_k = \{x_j \mid j = 1,\ldots,k,\ x_j \in Y\}, \quad k = 0,1,\ldots,D.$$

  - The selected features subset is initialized as an empty set $X_0 = 0$ with no features selected (*k*=0).
  - Halting occurs when *k* reaches the required number of selected features (k = 10).
  - The SFFS algorithm proceeds via two steps.
  - 'Inclusion' step and 'Conditional Exclusion' step.





# Methods

- SFFS algorithm
  - 'Inclusion' step
  - the most significant feature with respect to the currently selected feature set $X_k$, $x^+$ is determined: $x^+ = \arg\max_{x \in Y - X_k} J(X_k + x)$.
  - This feature is added to the selected features subset $X_{k+1} = X_k + x^+$ and the feature count incremented accordingly *k*=*k*+1
  - 'Conditional Exclusion' step
  - the least significant feature, $x^-$, of the current selected features subset is determined: $x^- = \arg\max_{x \in X_k} J(X_k - x)$.
  - The least significant feature is removed from the current selected feature set, $X_{k-1} = X_k - x^-$, the feature count is decremented, *k*=*k*-1
  - and the conditional exclusion stage is repeated.
  - if no improvement in discrimination be found, the algorithm returns to the inclusion step.
  - Search terminated at 10 features (k = 10).
  - The function *J* maximized was mean classification accuracy achieved by LDA (10-fold cross-validation)

# Methods

- To analyze that which electrode positions and frequency bands were used. They have used electrode maps for different tasks.
- Cross subject electrode frequency(# of counts)
  - electrode site was selected multiple times during a search based on differing features,
  - i.e. a single channel selected at differing frequency bands,
  - each instance would contribute independently towards an electrode frequency count.
- Cross subject electrode maps
  - To visualize the distribution of channels selected across subjects gradient maps are produced based on the frequency count of channels selected.
  - subject group gradient maps of selected channels are obtained by smoothing frequency counts over all channels.





# Methods

- Localization with sLORETA
  - To obtain localization results, we used Standardised Low Resolution Brain Electromagnetic Tompography (sLORETA) *[Pascual-Marqui, 2002].*
  - sLORETA is a linear method of computing a statistical map from EEG data which indicates the location of underlying source processes with less error.
  - Underlying sources providing spatial activation with closest correspondence to electrodes selected through feature selection were selected.

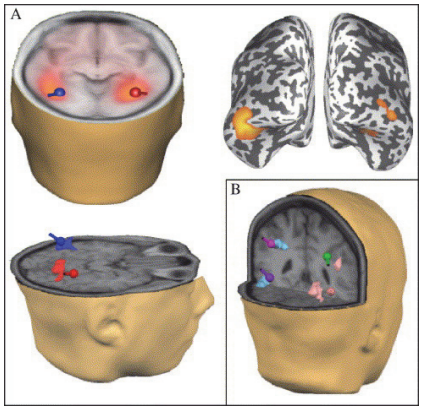

# Results

- Classification results derived through cross subject electrode selection are presented in parallel with source localization results.
- Based on activations derived from localization results we obtain closest match Brodmann area and attempt to identify neural structures

1. Motor imagery (left hand)

**Table 1**
Motor imagery (left hand): frequency of channels selected, ranked descending. Left group features based on band power. Right group features based on reflection coefficients. Highlighting: band power channels highlighted reflect channels in proximity to C4. Reflection coefficient channels highlighted reflect channels in proximity to C4.

| Band power | | | | | | Reflection coefficients | | | | | |
|---|---|---|---|---|---|---|---|---|---|---|---|
| Site | Freq. | % | Site | Freq. | % | Site | Freq. | % | Site | Freq. | % |
| **C4** | **32** | **8.74** | CP3 | 8 | 2.19 | **CP6** | **25** | **6.98** | **CP4** | **8** | **2.23** |
| P9 | 26 | 7.1 | Iz | 7 | 1.91 | **CP2** | **25** | **6.98** | P10 | 8 | 2.23 |
| AF7 | 19 | 5.19 | **FC6** | **7** | **1.91** | **C4** | **24** | **6.70** | P04 | 8 | 2.23 |
| Cz | 17 | 4.64 | P6 | 7 | 1.91 | P9 | 23 | 6.42 | P3 | 7 | 1.96 |
| P04 | 16 | 4.37 | AF3 | 6 | 1.64 | F3 | 17 | 4.75 | PO7 | 7 | 1.96 |
| **C2** | **14** | **3.83** | FC1 | 6 | 1.64 | **C2** | **16** | **4.47** | P4 | 7 | 1.96 |
| **CP6** | **14** | **3.84** | C3 | 6 | 1.64 | P8 | 15 | 4.19 | AF3 | 6 | 1.68 |
| P8 | 13 | 3.55 | O1 | 6 | 1.64 | **FC6** | **14** | **3.91** | AFz | 6 | 1.68 |
| PO7 | 12 | 3.28 | Pz | 6 | 1.64 | CP3 | 13 | 3.63 | FC5 | 5 | 1.4 |
| AF4 | 11 | 3.01 | F7 | 5 | 1.37 | Fp1 | 10 | 2.79 | CP1 | 5 | 1.4 |
| F8 | 11 | 3.01 | C1 | 5 | 1.37 | FC3 | 10 | 2.79 | AF4 | 4 | 1.12 |
| **CP4** | **11** | **3.01** | TP7 | 5 | 1.37 | C1 | 10 | 2.79 | F2 | 4 | 1.12 |
| P10 | 11 | 3.01 | P3 | 5 | 1.37 | CP5 | 10 | 2.79 | T8 | 4 | 1.12 |
| P08 | 11 | 3.01 | POz | 5 | 1.37 | Cz | 10 | 2.79 | P2 | 4 | 1.12 |
| **FC2** | **10** | **2.73** | C6 | 5 | 1.37 | CPz | 9 | 2.51 | FC1 | 3 | 0.84 |
| AFz | 9 | 2.46 | P2 | 5 | 1.37 | AF8 | 9 | 2.51 | Fpz | 3 | 0.84 |
| TP8 | 9 | 2.46 | F5 | 3 | 0.82 | C6 | 9 | 2.51 | F6 | 3 | 0.84 |
| P4 | 9 | 2.46 | | | | F4 | 8 | 2.23 | | | |

- Table 1 shows the frequency of channels utilized in discrimination of motor imagery of the left hand from idle activity





# Results

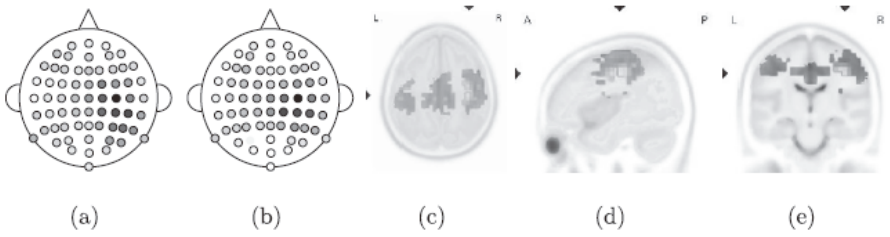


**Fig. 3.** Motor imagery (left hand). (a) and (b) Gradient maps based on frequency of channels selected by SFFS across subjects. Results based on band power and reflection coefficients, respectively. Darker colour indicates increased frequency. (c)–(e) sLORETA source localisation results corresponding to activation in Brodmann area 4 in the upper alpha/mu band (10.5–12 Hz).

- Fig. 3(a) and (b) shows gradient maps, obtained using band power and reflection coefficients based on the values outlined in Table 1
- For both feature representations electrode C4 achieves the highest frequency value
- Fig. 3(c)–(e) shows localization results with activation most similar to activity displayed in gradient maps.
- The closest match Brodmann area is BA4, the primary motor cortex, located on the precentral gyrus.
- This localization activity was found in the upper alpha/mu band (10.5–12 Hz)

# Results

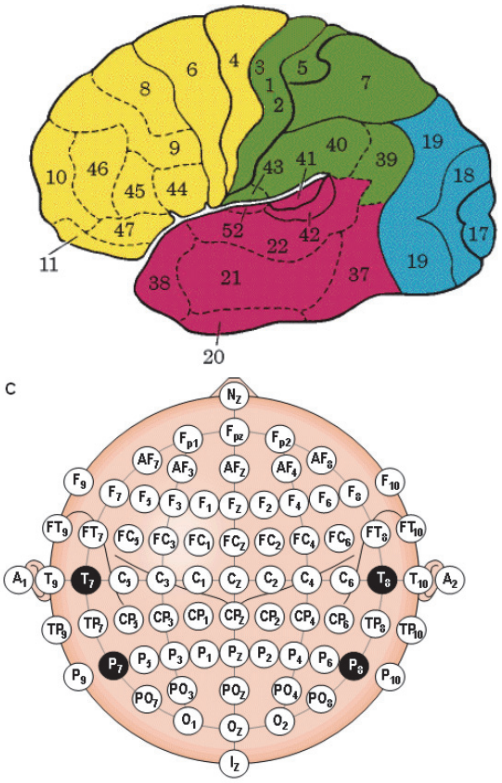


Functional Areas of the Brain

| Function | Brodmann Area |
|---|---|
| Vision | |
| primary | 17 |
| secondary | 18, 19, 20, 21, 37 |
| Audition | |
| primary | 41 |
| secondary | 22, 42 |
| Body Sensation | |
| primary | 1, 2, 3 |
| secondary | 5, 7 |
| Sensation, tertiary | 7, 22, 37, 39, 40 |
| Motor | |
| primary | 4 |
| secondary | 6 |
| eye mov't | 8 |
| speech | 44 |
| Motor, tertiary | 9, 10, 11, 45, 46, 47 |




- A Brodmann area is a region of the cerebral cortex defined based on its cytoarchitectonics(세포구축), or structure and organization of neurons.





# Results

## 2. Motor imagery (right hand)

**Table 2**
Motor imagery (right hand): frequency of channels selected, ranked descending. Left group features based on band power. Right group features based on reflection coefficients. Highlighting: band power channels highlighted reflect channels in proximity to CP1. Reflection coefficient channels highlighted reflect channels in proximity to CP3.

| Band power | | | | | | Reflection coefficients | | | | | |
|---|---|---|---|---|---|---|---|---|---|---|---|
| Site | Freq. | % | Site | Freq. | % | Site | Freq. | % | Site | Freq. | % |
| **CP3** | **27** | **7.20** | FT7 | 8 | 2.13 | **CP3** | **42** | **12.35** | CPz | 7 | 2.06 |
| P9 | 26 | 6.93 | PO7 | 8 | 2.13 | P8 | 19 | 5.59 | Fp2 | 7 | 2.06 |
| **CP1** | **24** | **6.40** | AFz | 8 | 2.13 | FC6 | 18 | 5.29 | F8 | 7 | 2.06 |
| Iz | 23 | 6.13 | F4 | 8 | 2.13 | C4 | 16 | 4.71 | CP6 | 7 | 2.06 |
| **C3** | **20** | **5.33** | O1 | 7 | 1.87 | FC5 | 15 | 4.41 | **C3** | **6** | **1.76** |
| Oz | 18 | 4.80 | O2 | 7 | 1.87 | **C5** | **13** | **3.82** | PO3 | 6 | 1.76 |
| P8 | 17 | 4.53 | F1 | 5 | 1.33 | AF8 | 13 | 3.82 | F4 | 5 | 1.47 |
| C6 | 16 | 4.27 | Fpz | 5 | 1.33 | C6 | 11 | 3.24 | P6 | 5 | 1.47 |
| P6 | 16 | 4.27 | F8 | 5 | 1.33 | FT7 | 10 | 2.94 | TP7 | 4 | 1.18 |
| **Cz** | **15** | **4.00** | AF4 | 4 | 1.07 | C2 | 10 | 2.94 | FCz | 4 | 1.18 |
| FC3 | 13 | 3.47 | **C1** | **3** | **0.80** | F3 | 9 | 2.65 | **P3** | **3** | **0.88** |
| F5 | 10 | 2.67 | T7 | 3 | 0.80 | F7 | 9 | 2.65 | **P5** | **3** | **0.88** |
| C5 | 10 | 2.67 | AF8 | 3 | 0.80 | FC3 | 9 | 2.65 | O1 | 3 | 0.88 |
| **P3** | **10** | **2.67** | FC6 | 3 | 0.80 | Oz | 9 | 2.65 | AFz | 3 | 0.88 |
| **Pz** | **10** | **2.67** | TP7 | 2 | 0.53 | P10 | 9 | 2.65 | **CP5** | **2** | **0.59** |
| CP4 | 10 | 2.67 | P7 | 1 | 0.27 | P08 | 9 | 2.65 | CP4 | 2 | 0.59 |
| POz | 9 | 2.40 | **CPz** | **1** | **0.27** | Fp1 | 8 | 2.35 | P04 | 2 | 0.59 |
| Fp2 | 9 | 2.40 | F6 | 1 | 0.27 | **P1** | **8** | **2.35** | F5 | 1 | 0.29 |
| C2 | 9 | 2.40 | C4 | 1 | 0.27 | Cz | 8 | 2.35 | FC1 | 1 | 0.29 |
| | | | | | | CP2 | 8 | 2.35 | FC4 | 1 | 0.29 |
| | | | | | | AF7 | 7 | 2.06 | T8 | 1 | 0.29 |

- Table 2 shows the frequency of channels utilized in discrimination of motor imagery of the right hand from idle activity

# Results

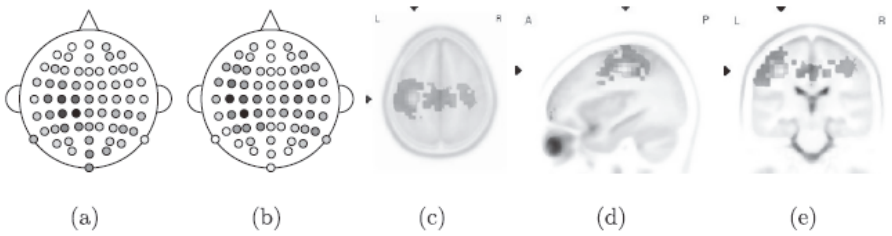


**Fig. 4.** Motor imagery (right hand). (a) and (b) Gradient maps based on frequency of channels selected by SFFS across subjects. Results based on band power and reflection coefficients, respectively. Darker colour indicates increased frequency. (c)–(e) sLORETA source localisation results corresponding to activation in Brodmann area 3 in the upper alpha/mu band (10.5–12 Hz).

- Fig. 4(a) and (b) shows gradient maps, obtained using band power and reflection coefficients based on the values outlined in Table 2
- For both feature representations electrode CP3(near the C3) achieves the highest frequency value
- Fig. 4(c)–(e) shows localization results with activation most similar to activity displayed in gradient maps (a) and(b).
- The closest match Brodmann area is BA3 located on the primary somatosensory cortex
- This localization activity was found in the upper alpha/mu band (10.5–12 Hz)





# Results

3. Auditory recall

**Table 3**
Auditory recall: frequency of channels selected, ranked descending. Left group features based on band power. Right group features based on reflection coefficients. Highlighting: band power channels highlighted reflect channels in proximity to TP8. Reflection coefficient channels highlighted in regular bold reflect channels in proximity to CP6, channels highlighted in italic bold reflect channels in proximity to F4.

| Band power | | | | | | Reflection coefficients | | | | | |
|---|---|---|---|---|---|---|---|---|---|---|---|
| Site | Freq. | % | Site | Freq. | % | Site | Freq. | % | Site | Freq. | % |
| **P10** | **19** | **6.25** | C6 | 5 | 1.64 | ***AF8*** | ***24*** | ***7.16*** | Fz | 8 | 2.39 |
| **CP6** | **18** | **5.92** | P08 | 5 | 1.64 | ***AFz*** | ***20*** | ***5.97*** | ***FC6*** | ***8*** | ***2.39*** |
| Fp1 | 16 | 5.26 | CP5 | 4 | 1.32 | ***F4*** | ***19*** | ***5.67*** | ***FC4*** | ***7*** | ***2.09*** |
| P7 | 15 | 4.93 | P1 | 4 | 1.32 | FC1 | 17 | 5.07 | **CP4** | **7** | **2.09** |
| F5 | 14 | 4.61 | P5 | 4 | 1.32 | CP6 | 17 | 5.07 | FT8 | 6 | 1.79 |
| F7 | 13 | 4.28 | Iz | 4 | 1.32 | CP3 | 14 | 4.18 | Cz | 6 | 1.79 |
| **TP8** | **13** | **4.28** | POz | 4 | 1.32 | **TP8** | **13** | **3.88** | F1 | 5 | 1.49 |
| F1 | 11 | 3.62 | Pz | 4 | 1.32 | **P4** | **13** | **3.88** | Fpz | 5 | 1.49 |
| AF8 | 10 | 3.29 | Oz | 3 | 0.99 | F3 | 12 | 3.58 | **T8** | **5** | **1.49** |
| C5 | 9 | 2.96 | Fz | 3 | 0.99 | T7 | 12 | 3.58 | P10 | 5 | 1.49 |
| Fp2 | 9 | 2.96 | FC4 | 3 | 0.99 | ***AF4*** | ***12*** | ***3.58*** | AF3 | 4 | 1.19 |
| AFz | 9 | 2.96 | Cz | 3 | 0.99 | P08 | 12 | 3.58 | P5 | 4 | 1.19 |
| FC2 | 9 | 2.96 | P8 | 3 | 0.99 | C3 | 11 | 3.28 | CP2 | 4 | 1.19 |
| CP2 | 9 | 2.96 | F3 | 2 | 0.66 | **C6** | **10** | **2.99** | FT7 | 3 | 0.9 |
| 02 | 9 | 2.96 | FT7 | 2 | 0.66 | FC3 | 9 | 2.69 | F7 | 2 | 0.6 |
| C4 | 8 | 2.63 | FCz | 2 | 0.66 | P1 | 9 | 2.69 | P04 | 2 | 0.6 |
| **P6** | **8** | **2.63** | P2 | 2 | 0.66 | ***F6*** | ***9*** | ***2.69*** | Fp1 | 1 | 0.3 |
| TP7 | 7 | 2.30 | AF3 | 1 | 0.33 | **C4** | **9** | **2.69** | CPz | 1 | 0.3 |
| **T8** | **7** | **2.30** | CP3 | 1 | 0.33 | **P6** | **9** | **2.69** | Fp2 | 1 | 0.3 |
| PO3 | 6 | 1.97 | CPz | 1 | 0.33 | | | | | | |
| F2 | 6 | 1.97 | FT8 | 1 | 0.33 | | | | | | |
| P04 | 6 | 1.97 | C2 | 1 | 0.33 | | | | | | |
| P9 | 5 | 1.64 | CP4 | 1 | 0.33 | | | | | | |
| F6 | 5 | 1.64 | | | | | | | | | |

- Table 3 lists the frequency of channels used in the discrimination of auditory imagery from idle activity

# Results

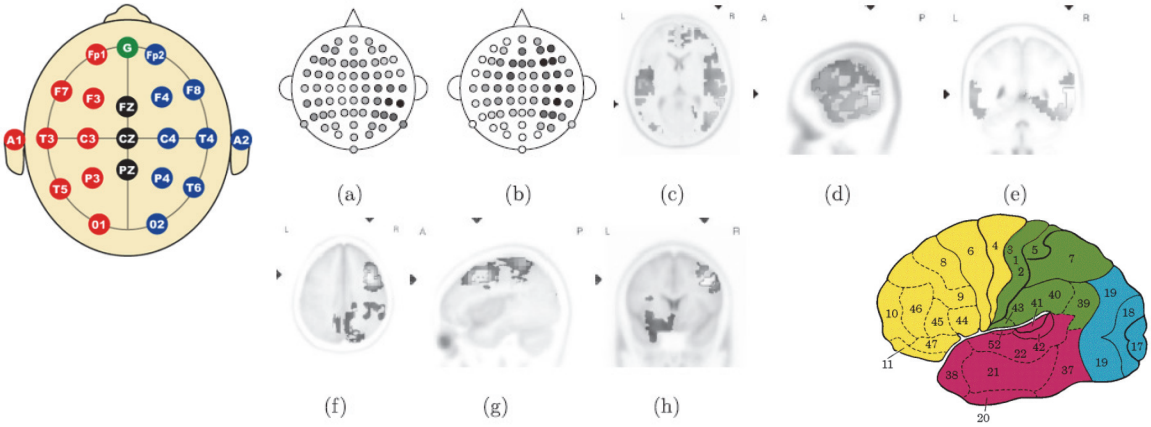


**Fig. 5.** Auditory recall. (a) and (b) Gradient maps based on frequency of channels selected by SFFS across subjects. Results based on band power and reflection coefficients, respectively. Darker colour indicates increased frequency. (c)–(e) sLORETA source localisation results corresponding to activation in Brodmann area 21 in the high beta (21–30 Hz) range. (f)–(h) sLORETA source localisation results corresponding to activation in Brodmann area 9 in the lower alpha band (8.5–10 Hz).

- Fig. 5(a), the gradient map based on band power, has greatest density of channels selected around TP8
- Fig. 5(b), show a primary area of main density around electrode CP6 with a secondary area commonly selected around FP4
- Fig. 5(c)–(e) has closest match in Brodmann area 21 located in the middle temporal gyrus (high beta (21–30 Hz) range).
- Fig. 5(f)–(h) has closest match is Brodmann area 9 on the precentral gyrus (lower alpha band (8.5–10 Hz)).





# Results

## 4. Phone imagery

**Table 4**
Phone imagery: frequency of channels selected, ranked descending. Left group features based on band power. Right group features based on reflection coefficients. Highlighting: band power channels highlighted in regular bold reflect channels in proximity to C6, channels highlighted in italic bold reflect channels in proximity to FC5. Reflection coefficient channels highlighted in regular bold reflect channels in proximity to TP7, channels highlighted in italic bold reflect channels in proximity to CP6.

| Band power | | | | | | Reflection coefficients | | | | | |
|---|---|---|---|---|---|---|---|---|---|---|---|
| Site | Freq. | % | Site | Freq. | % | Site | Freq. | % | Site | Freq. | % |
| AF4 | 23 | 6.55 | P5 | 7 | 1.99 | **P9** | **27** | **7.20** | P10 | 9 | 2.4 |
| AF8 | 20 | 5.70 | P7 | 7 | 1.99 | AF7 | 26 | 6.93 | C3 | 8 | 2.13 |
| **C6** | **19** | **5.41** | Pz | 7 | 1.99 | ***T8*** | ***20*** | ***5.33*** | **P7** | **8** | **2.13** |
| FCz | 18 | 5.13 | P2 | 6 | 1.71 | ***P8*** | ***19*** | ***5.07*** | F8 | 8 | 2.13 |
| **T8** | **16** | **4.56** | P04 | 6 | 1.71 | **P5** | **18** | **4.80** | F3 | 7 | 1.87 |
| ***F7*** | ***14*** | ***3.99*** | ***F3*** | ***5*** | ***1.42*** | Fp2 | 17 | 4.53 | CPz | 7 | 1.87 |
| ***T7*** | ***14*** | ***3.99*** | ***FC5*** | ***5*** | ***1.42*** | AF8 | 15 | 4 | P2 | 7 | 1.87 |
| CP5 | 14 | 3.99 | P9 | 5 | 1.42 | **CP5** | **14** | **3.73** | O1 | 6 | 1.6 |
| **C4** | **14** | **3.99** | 02 | 5 | 1.42 | Fpz | 13 | 3.47 | P1 | 5 | 1.33 |
| ***C5*** | ***13*** | ***3.70*** | Fp1 | 4 | 1.14 | FT7 | 12 | 3.2 | FT8 | 5 | 1.33 |
| Iz | 12 | 3.42 | AF7 | 4 | 1.14 | **T7** | **12** | **3.20** | ***C6*** | ***5*** | ***1.33*** |
| **CP4** | **11** | **3.13** | Fp2 | 3 | 0.85 | ***P4*** | ***12*** | ***3.20*** | ***P6*** | ***5*** | ***1.33*** |
| PO7 | 10 | 2.85 | AFz | 3 | 0.85 | Pz | 12 | 3.2 | Iz | 4 | 1.07 |
| **FT8** | **10** | **2.85** | Cz | 3 | 0.85 | 2 | 12 | 3.2 | FC2 | 4 | 1.07 |
| **CP6** | **10** | **2.85** | C2 | 3 | 0.85 | CP1 | 10 | 2.67 | Cz | 4 | 1.07 |
| P10 | 10 | 2.85 | Oz | 2 | 0.57 | P04 | 10 | 2.67 | C2 | 3 | 0.8 |
| P8 | 9 | 2.56 | **FC6** | **2** | **0.57** | **TP7** | **9** | **2.40** | CP2 | 3 | 0.8 |
| ***F5*** | ***8*** | ***2.28*** | CP2 | 2 | 0.57 | ***C4*** | ***9*** | ***2.40*** | POz | 1 | 0.27 |
| ***FT7*** | ***8*** | ***2.28*** | AF3 | 1 | 0.28 | ***TP8*** | ***9*** | ***2.40*** | | | |
| C1 | 8 | 2.28 | P1 | 1 | 0.28 | | | | | | |
| Fz | 8 | 2.28 | CPz | 1 | 0.28 | | | | | | |

- Table 4 lists the frequency of channels used in the discrimination of phone imagery from idle activity

# Results

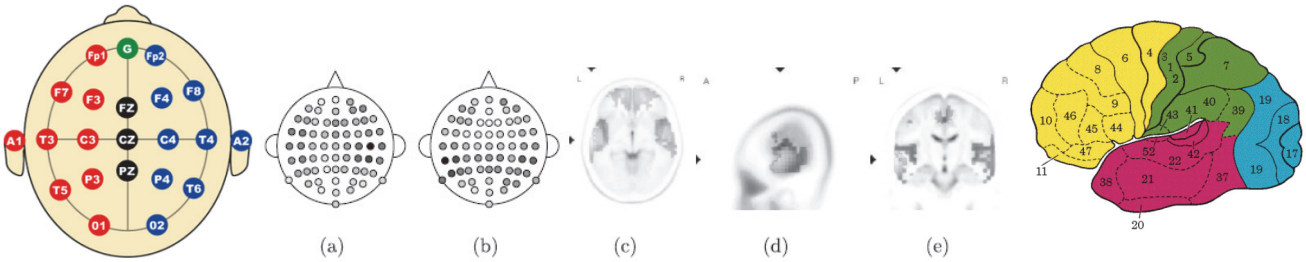


Fig. 6. Phone imagery. (a) and (b) Gradient maps based on frequency of channels selected by SFFS across subjects. Results based on band power and reflection coefficients, respectively. Darker colour indicates increased frequency. (c)–(e) sLORETA source localisation results corresponding to activation in Brodmann area 21 in the mid beta (18.5–21 Hz) range.

- Fig. 6(a), the gradient map based on band power, has greatest density of channels selected around C6, secondary area surrounding FC5.
- Fig. 6(b) which has two areas of density centered around TP7 and CP6
- Fig. 6(c)–(e) shows localization results which best explain the pattern of activation found in gradient maps (Fig. 6(a) and (b)).
- Closest match Brodmann area is BA21 located on the middle temporal gyrus (freq. : mid beta (18.5–21 Hz) range).
- In comparison to the auditory recall results shown in Figs. 5(a) and (b), Figs. 6(a) and (b) show a greater degree of bilateral activity.





# Results

## 5. Arithmetic

**Table 5**
Arithmetic: frequency of channels selected, ranked descending. Left group features based on band power. Right group features based on reflection coefficients. Highlighting: band power channels highlighted reflect channels in proximity to AF3. Reflection coefficient channels highlighted reflect channels in proximity to CP4.

| Band power | | | | | | Reflection coefficients | | | | | |
|---|---|---|---|---|---|---|---|---|---|---|---|
| Site | Freq. | % | Site | Freq. | % | Site | Freq. | % | Site | Freq. | % |
| P9 | 28 | 7.89 | FC5 | 6 | 1.69 | **P6** | **24** | **6.40** | T8 | 8 | 2.13 |
| P10 | 21 | 5.92 | PO3 | 6 | 1.69 | P9 | 19 | 5.07 | **CP4** | **7** | **1.87** |
| **F3** | **20** | **5.63** | Iz | 6 | 1.69 | CP3 | 16 | 4.27 | **CP6** | **6** | **1.60** |
| **F5** | **19** | **5.35** | **AFz** | **6** | **1.69** | FC1 | 15 | 4 | P8 | 6 | 1.6 |
| CP2 | 18 | 5.07 | F4 | 6 | 1.69 | AF3 | 14 | 3.73 | 2 | 6 | 1.6 |
| **AF3** | **13** | **3.66** | POz | 5 | 1.41 | F5 | 13 | 3.47 | FC5 | 5 | 1.33 |
| C5 | 13 | 3.66 | FT8 | 5 | 1.41 | **C6** | **13** | **3.47** | POz | 5 | 1.33 |
| Fp2 | 13 | 3.66 | CP5 | 4 | 1.13 | TP8 | 13 | 3.47 | Fpz | 5 | 1.33 |
| TP8 | 11 | 3.10 | FC2 | 4 | 1.13 | F8 | 12 | 3.2 | F4 | 5 | 1.33 |
| **Fp1** | **10** | **2.82** | FCz | 4 | 1.13 | C3 | 11 | 2.93 | FT8 | 5 | 1.33 |
| **AF7** | **10** | **2.82** | T8 | 4 | 1.13 | AF4 | 11 | 2.93 | **P4** | **5** | **1.33** |
| T7 | 10 | 2.82 | P08 | 4 | 1.13 | F7 | 10 | 2.67 | Fp1 | 4 | 1.07 |
| C2 | 10 | 2.82 | TP7 | 3 | 0.85 | F2 | 10 | 2.67 | FT7 | 4 | 1.07 |
| 02 | 10 | 2.82 | P3 | 3 | 0.85 | FCz | 10 | 2.67 | P1 | 4 | 1.07 |
| C3 | 9 | 2.54 | P7 | 3 | 0.85 | **C2** | **10** | **2.67** | PO7 | 4 | 1.07 |
| P1 | 9 | 2.54 | AF4 | 3 | 0.85 | **P2** | **10** | **2.67** | Fp2 | 3 | 0.8 |
| Oz | 9 | 2.54 | F8 | 3 | 0.85 | CP5 | 9 | 2.4 | F6 | 3 | 0.8 |
| Pz | 9 | 2.54 | **F1** | **2** | **0.56** | O1 | 9 | 2.4 | P08 | 3 | 0.8 |
| CP3 | 8 | 2.25 | F2 | 2 | 0.56 | AF8 | 9 | 2.4 | P5 | 2 | 0.53 |
| AF8 | 8 | 2.25 | F7 | 1 | 0.28 | **CP2** | **9** | **2.40** | CPz | 2 | 0.53 |
| Fz | 8 | 2.25 | FC1 | 1 | 0.28 | F1 | 8 | 2.13 | FC6 | 2 | 0.53 |
| **Fpz** | **7** | **1.97** | C1 | 1 | 0.28 | FC3 | 8 | 2.13 | TP7 | 1 | 0.27 |
| | | | | | | T7 | 8 | 2.13 | Oz | 1 | 0.27 |
| | | | | | | FC4 | 8 | 2.13 | | | |

- Table 5 lists the frequency of channels used in the discrimination of arithmetic from idle activity
- Table 5 shows greatest frequency at AF3 for band power features, and at CP4 when discrimination is based on reflection coefficients.

# Results

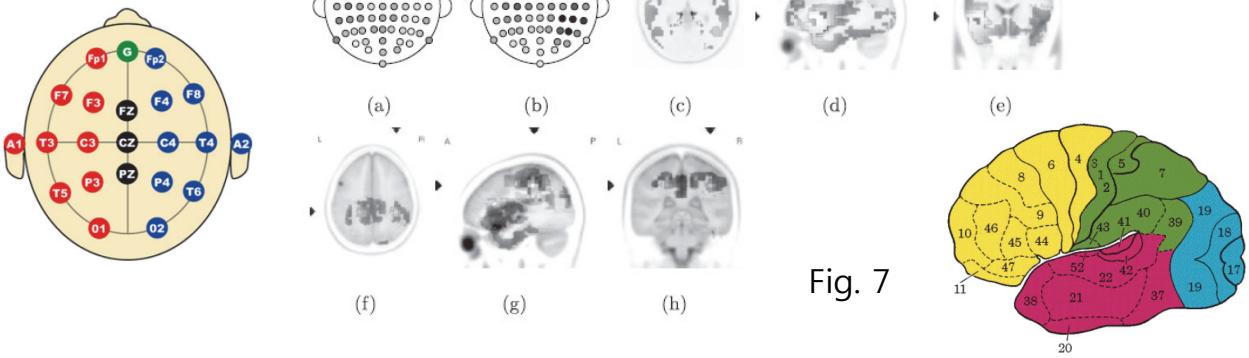


Fig. 7



- Arithmetic mental activity shows distinct differences in classification areas obtained dependent on feature extraction method, band power and AR coefficients.
- Fig. 7(c)–(e) and Fig. 7(f)–(h) represent areas of activation best describing patterns of activation found with Fig. 7(a) and Fig. 7(b) respectively .
- The closest match Brodmann area related to activation was BA46 in the inferior frontal gyrus of the left hemisphere (low beta band (12.5–18 Hz)).
- Fig. 7(f)–(h) shows activation centered on Brodmann area 40, inferior parietal lobe, in the area of the supramarginal gyrus (theta band (6.5–8 Hz)).





# Results

## 6. Navigation

**Table 6**
Navigation imagery: frequency of channels selected, ranked descending. Left group features based on band power. Right group features based on reflection coefficients. Highlighting: band power channels highlighted in regular bold reflect channels in proximity to AF4, channels highlighted in italic bold reflect channels in proximity to CP2. Reflection coefficient channels highlighted in regular bold reflect channels in proximity to PO4, channels highlighted in italic bold reflect channels in proximity to AFz.

| Band power | | | | | | Reflection coefficients | | | | | |
|---|---|---|---|---|---|---|---|---|---|---|---|
| Site | Freq. | % | Site | Freq. | % | Site | Freq. | % | Site | Freq. | % |
| F7 | 20 | 6.04 | C6 | 8 | 2.42 | **P04** | **37** | **9.61** | FC1 | 7 | 1.82 |
| **AF4** | **18** | **5.44** | P8 | 8 | 2.42 | CP1 | 26 | 6.75 | CP3 | 7 | 1.82 |
| F2 | 18 | 5.44 | Iz | 7 | 2.11 | ***AFz*** | ***21*** | ***5.45*** | F4 | 7 | 1.82 |
| Fp1 | 17 | 5.14 | **Fpz** | 7 | **2.11** | **CP2** | **20** | **5.19** | FCz | 7 | 1.82 |
| ***CP2*** | ***17*** | ***5.14*** | **F6** | 7 | **2.11** | F6 | 18 | 4.68 | Iz | 6 | 1.56 |
| ***P1*** | ***16*** | ***4.83*** | CP3 | 6 | 1.81 | **P2** | 17 | **4.42** | **P08** | **6** | **1.56** |
| T8 | 16 | 4.83 | F8 | 6 | 1.81 | FT7 | 16 | 4.16 | FC6 | 5 | 1.3 |
| ***CP1*** | ***14*** | ***4.23*** | T7 | 5 | 1.51 | FT8 | 16 | 4.16 | **CP6** | **5** | **1.30** |
| AF8 | 13 | 3.93 | Oz | 5 | 1.51 | ***Fpz*** | ***15*** | ***3.90*** | F5 | 4 | 1.04 |
| P04 | 13 | 3.93 | C4 | 5 | 1.51 | ***Fp2*** | ***12*** | ***3.12*** | ***F2*** | ***4*** | ***1.04*** |
| P08 | 12 | 3.63 | P4 | 5 | 1.51 | ***Fz*** | ***11*** | ***2.86*** | TP7 | 3 | 0.78 |
| P7 | 11 | 3.32 | F3 | 4 | 1.21 | ***F1*** | ***10*** | ***2.60*** | PO7 | 3 | 0.78 |
| **AFz** | **11** | **3.32** | FC3 | 4 | 1.21 | C4 | 10 | 2.6 | F8 | 3 | 0.78 |
| F5 | 10 | 3.02 | CP5 | 4 | 1.21 | P1 | 9 | 2.34 | **P4** | **3** | **0.78** |
| FT7 | 9 | 2.72 | **Fp2** | **4** | **1.21** | PO3 | 9 | 2.34 | P6 | 3 | 0.78 |
| ***C2*** | ***9*** | ***2.72*** | FT8 | 3 | 0.91 | TP8 | 9 | 2.34 | ***AF3*** | ***2*** | ***0.52*** |
| ***P2*** | ***9*** | ***2.72*** | ***C1*** | ***2*** | ***0.60*** | F3 | 8 | 2.08 | CPz | 2 | 0.52 |
| P5 | 8 | 2.42 | | | | FC5 | 8 | 2.08 | AF7 | 1 | 0.26 |
| | | | | | | T7 | 8 | 2.08 | C5 | 1 | 0.26 |
| | | | | | | POz | 8 | 2.08 | O1 | 1 | 0.26 |
| | | | | | | FC4 | 8 | 2.08 | C2 | 1 | 0.26 |
| | | | | | | FC3 | 7 | 1.82 | C6 | 1 | 0.26 |

- Table 6 lists the frequency of channels used in the discrimination of navigation imagery from idle activity

# Results

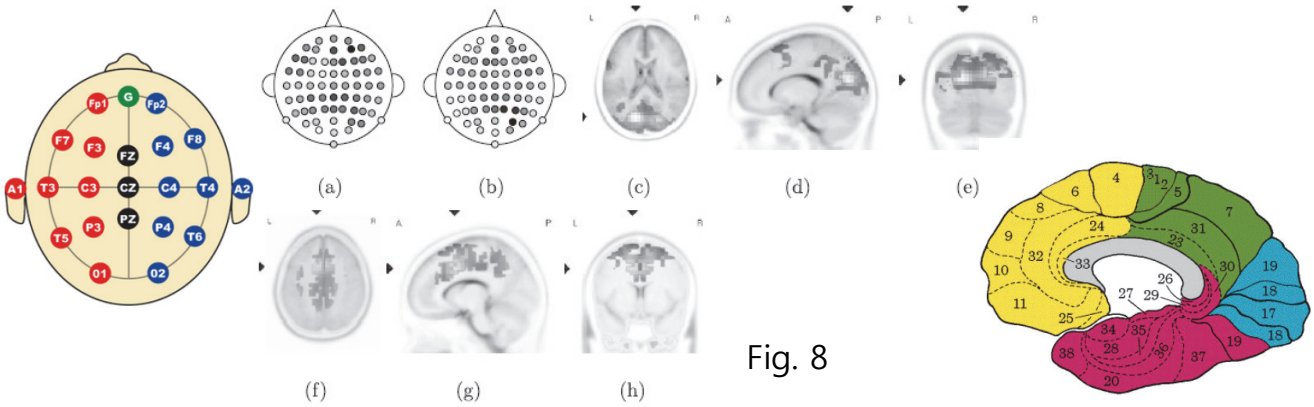


Fig. 8

- Fig. 8(a) shows gradient maps produced from band power features, the greatest density value is centered around AF4 with a second area of increased density located around CP2.
- The equivalent values for Fig. 8(b) are centered at PO4 and AFz.
- Activity centered around CP2 in the case of band power, and PO4 in the case of reflection coefficients is best matched by localization activity shown in Fig. 8(c)–(e).
- The closest matched Brodmann area is BA31, on the parietal lobe in the mid beta band(18.5–21Hz).
- Frontal activation found in Fig. 8(a) and (b), centered around AF4 and AFz is best matched by Fig. 8(f)–(h) in the lower beta band (12.5–18 Hz) at Brodmann area BA32.





# Results

Contrast of feature distributions

- they calculate the relative overlap in spatial electrode distributions using two methods.

1. dot product of feature vectors
   - The values in Table 7 show the dot product of feature vectors divided over a fixed electrode count of 64.
   - Higher values indicate greater overlap in the cross subject distribution maps
   - The lowest levels of overlap are associated with contrasts of the distributions produced by motor imagery tasks
   - The highest degree of overlap is found between the auditory imagery and arithmetic task based on reflection coefficients

**Table 7**
Comparative overlap in spatial electrode distributions: the dot product of normalised electrode distribution vectors, divided over electrode count. Greater values indicate increased overlap. Highlighting: values in italic are based on band power features. Values in standard text are based on reflection coefficients.

| Tasks | MoIm:Left | MoIm:Right | Navigation | Arithmetic | Auditory | Phone |
|---|---|---|---|---|---|---|
| MoIm:Left | | 0.06 | 0.06 | 0.09 | 0.11 | 0.07 |
| MoIm:Right | *0.07* | | 0.11 | 0.11 | 0.10 | 0.11 |
| Navigation | *0.08* | *0.07* | | 0.16 | 0.15 | 0.10 |
| Arithmetic | *0.08* | *0.08* | *0.12* | | 0.17 | 0.16 |
| Auditory | *0.07* | *0.06* | *0.10* | *0.11* | | 0.16 |
| Phone | *0.10* | *0.10* | *0.14* | *0.13* | *0.14* | |

# Results

Contrast of feature distributions

2. distance between the density of features

- The values in Table 8 are the summed absolute distance between paired feature vectors
- providing a measure of the difference in density distributions of features for contrasted cognitive tasks
- The greatest distance in Table 8 is found between motor imagery of the left hand and arithmetic in the band power domain
- The lowest distance, is found between the auditory imagery and arithmetic tasks based on reflection coefficients.

**Table 8**
Comparative distance between electrode feature density vectors: the sum of absolute distance between electrode distribution vectors. Lower values indicate similarity in feature distribution. Highlighting: values in italic are based on band power features. Values in standard text are based on reflection coefficients.

| Tasks | MoIm:Left | MoIm:Right | Navigation | Arithmetic | Auditory | Phone |
|---|---|---|---|---|---|---|
| MoIm:Left | | 0.44 | 0.53 | 0.41 | 0.49 | 0.60 |
| MoIm:Right | *0.57* | | 0.46 | 0.44 | 0.47 | 0.50 |
| Navigation | *0.49* | *0.53* | | 0.39 | 0.44 | 0.59 |
| Arithmetic | *0.72* | *0.54* | *0.51* | | 0.31 | 0.47 |
| Auditory | *0.45* | *0.59* | *0.46* | *0.49* | | 0.68 |
| Phone | *0.52* | *0.58* | *0.41* | *0.53* | *0.36* | |





# Conclusions

- Primary centers of activity for motor imagery tasks are localized to the pre- and postcentral gyrus
- Auditory-based tasks show activity in the middle temporal gyrus
- Calculation activity was localized to the left inferior frontal gyrus and right supramarginal gyrus
- Navigation imagery produced activity in the praecuneus and anterior cingulate cortex.
- Spatial areas of activation suggest that arithmetic and auditory tasks show promise for pairwise discrimination based on single recording sites.
- sLORETA results suggest that motor imagery tasks will show greatest discrimination from baseline EEG activity(idle state)

# Thank you

**INFONET, GIST**
*Journal Club* (2013. 4. 30)

# Scanner-Free and Wide-Field Endoscopic Imaging by Using a Single Multimode Optical Fiber

Authors: Youngwoon Choi, Changhyeong Yoon, Moonseok Kim, Taeseok Daniel Yang, Christopher Fang-Yen, Ramachandra R. Dasari, Kyoung Jin Lee, and Wonshik Choi
Publication: Physical Review Letters, 109, 203901 (16 Nov. 2012)
Speaker: Hwanchol Jang

**Short summary:** An endoscopic method is developed to replace the fiber bundle scope by a single multimode fiber. The dispersion in a multimode fiber is reversed by TLI methods. The speckle patterns are reduced by averaging the object images with different speckle illuminations.

## I. OPTICAL FIBER FOR ENDOSCOPY

**Multimode optical fiber**
A multimode optical fiber has drawn interest because numerous independent spatial modes can be used for parallel information transport. However, the single multimode fiber could not be used in itself for the imaging purpose. When a light wave couples to and propagates through the fiber, the wave is distorted into a complex pattern because of mode dispersion.

**Mode dispersion**
Rays of light enter the fiber with different angles to the fiber axis, up to the fiber's acceptance angle. Rays that enter with a shallower angle travel by a more direct path, and arrive sooner than rays that enter at a steeper angle (which reflect many more times off the boundaries of the core as they travel the length of the fiber). The arrival of different components of the signal at different times distorts the shape.

Moreover, it has been much more challenging to use a single multimode fiber for practical endoscopic imaging in which the imaging operation should be performed in the reflection mode. In such a case, the light wave injected into the fiber is distorted twice, i.e., on the way in for the illumination and on the way out for the detection.

**Fiber scope**
For this reason, a fiber bundle has been widely used and thus became a standard for commercial endoscopes. In this fiber scope, each fiber constituting the bundle acts as a single pixel of an image, and the number of fibers in the bundle determines the pixel resolution.
Problem: Therefore, the requirement for a large number of fibers for high resolution imaging has posed constraints on the diameter of the endoscope, thereby causing considerable limitation on the accessibility of the device.

## II. PROPOSED LENSELESS MICROENDOSCOPY BY A SINGLE FIBER (LMSF)

The multimode fiber is converted into a self-contained 3D imaging device that does not require a scanner or a lens.

**Record the transmission matrix**
The authors make use of the measured transmission matrix of a multimode optical fiber to reverse the on-the-way-out distortion of the detected light.
The transmission matrix of an unknown complex medium was used for the delivery of an image through the medium. In fact, a multimode optical fiber can also be considered as a complex medium because bending and twisting of the fiber complicate wave propagation through the fiber.

**Speckle imaging method**
By employing the speckle imaging method, the on-the-way-in distortion was also eliminated.

## III. EXPERIMENTAL SET-UP

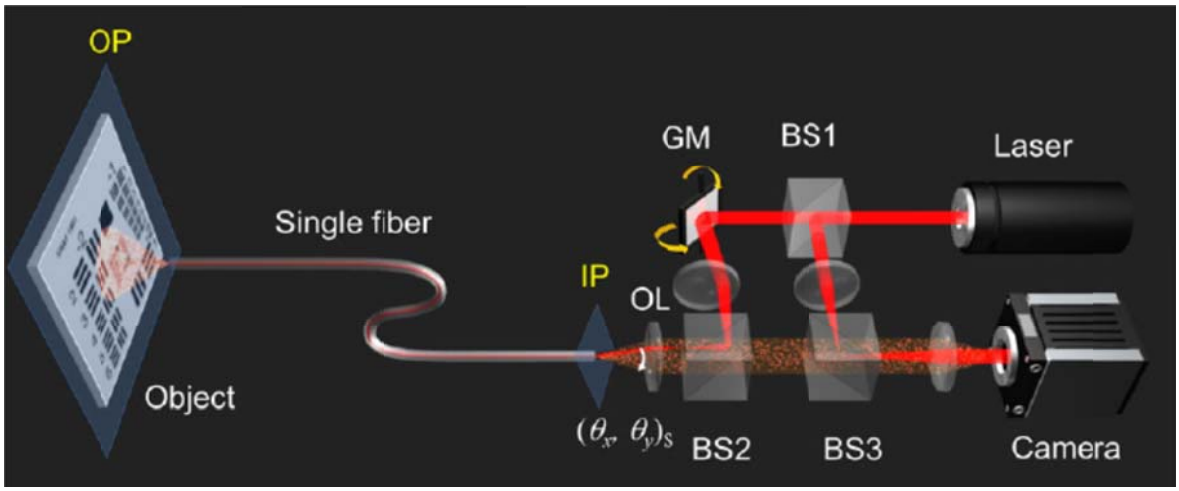


The beam illuminates at the input plane (IP) of the fiber, couples to the fiber, and subsequently propagates toward the object plane (OP) located at the exit of the fiber to illuminate a target object.
The laser beam reflected by BS1 is combined with the beam from the fiber to form an interference image at the camera. Using an off-axis digital holography algorithm, both amplitude and phase of the image from the fiber are retrieved.

## IV. TECHNIQUES FOR LMSF

**Two sources of the distortion**
Two processes mask the object information: (1) distortion of illumination light on the way in (IP to OP) and (2) the scrambling of the light reflected by the object on the way out (OP to IP). In

order to overcome these two distortions, they employ methods of speckle imaging and turbid lens imaging (TLI), respectively.

**Descrambling**

They first characterize the input-output response of the optical fiber from the object side to the camera side (OP to IP). They scan the incident wave in its angle $(\theta_\xi, \theta_\eta)_T$ to the fiber and record its transmitted image at the camera. A set of these angle-dependent transmission images is called the transmission matrix T. The transmission matrix elements are measured up to 0.22 NA by recording 15000 images.

Once the transmission matrix is recorded, an object image at the OP can be reconstructed from the distorted image recorded at the IP by using the TLI. The process is an inversion of the transmission matrix given by the relation EOP

$$E_{OP}(\xi,\eta) = T^{-1}E_{IP}(x,y)$$

Here EIP and $T^{-1}$ represent the recorded image at the IP and the inversion of the measured transmission matrix, respectively, and EOP is the image at the OP. Using Eq. (1), the distortion from OP to IP is reversed.

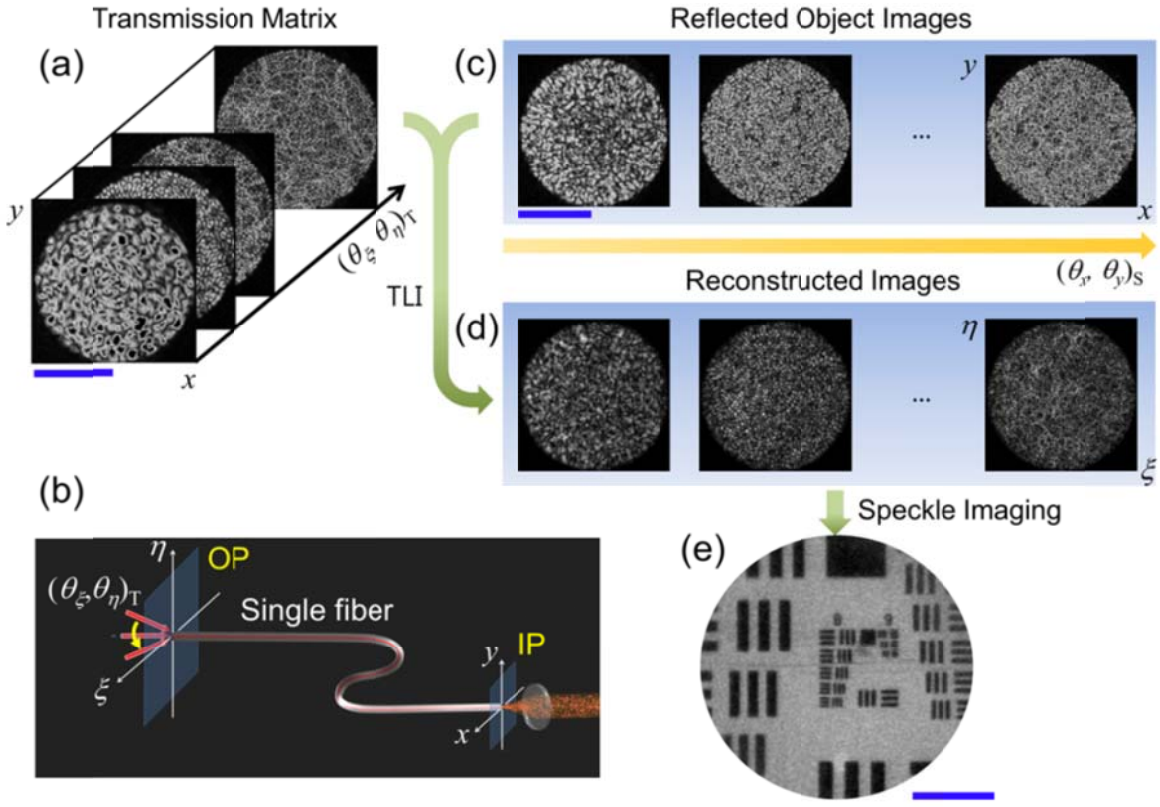


**Eliminating the speckle pattern**

The transmitted patterns are random speckles and the average size of the speckle decreases as the angle of illumination increases. This is because a high angle of illumination mostly couples to the high-order modes of the fiber.

The reconstructed images remain devoid of object structure because the illumination light is distorted due to the propagation of the illumination from IP to OP.
The change in the illumination angle causes the variation of the illumination light at the target object; in other words, a different speckle field is generated as we vary the angle $(\theta_x, \theta_y)_S$.

According to the speckle imaging method, a clean object image can be acquired if we average sufficient numbers of images recorded at different speckle illuminations.
The complex speckle illumination patterns are averaged out, leaving a clean object image.

**Scanning of the fiber end to enlarge the view field.**
They measured the transmission matrix of the fiber at an initial position of the fiber end and then used the same matrix to reconstruct object images taken while moving the fiber end.
Although bending induced by the movement of the fiber causes a change of the transmission matrix, many of the matrix elements stay intact and contribute to the image reconstruction.
According to their experiment, the LMSF is working well up to a centimeter-travel of the fiber end, confirming that LMSF has partial flexibility for searching for the view field.

## V. CONCLUSION

The same techniques used in turbid medium lens are employed to reverse the distortion of the multimode fiber.
The transmission matrix stays almost the same even with the centimeter changes of the fiber end.